UNIVERSIDADE ESTADUAL DE CAMPINAS
SISTEMA DE BIBLIOTECAS DA UNICAMP
REPOSITÓRIO DA PRODUÇÃO CIENTIFICA E INTELECTUAL DA UNICAMP

Versão do arquivo anexado / Version of attached file:

Versão do Editor / Published Version

Mais informações no site da editora / Further information on publisher's website:
https://www.sciencedirect.com/science/article/pii/S0264127518307950

DOI: 10.1016/j.matdes.2018.10.040

Direitos autorais / Publisher's copyright statement:
©2018 by Elsevier. All rights reserved.

DIRETORIA DE TRATAMENTO DA INFORMAÇÃO

Cidade Universitária Zeferino Vaz Barão Geraldo
CEP 13083-970 – Campinas SP
Fone: (19) 3521-6493
http://www.repositorio.unicamp.br

Materials and Design 160 (2018) 1186–1195

Contents lists available at ScienceDirect

Materials and Design

journal homepage: www.elsevier.com/locate/matdes

The effect of Zr and Sn additions on the microstructure of Ti-Nb-Fe gum metals with high elastic admissible strain

Mariana R. Dal Bó [a,1], Camilo A.F. Salvador [a,1], Mariana G. Mello [a], Dalton D. Lima [a], Guilherme A. Faria [b], Antonio J. Ramirez [b], Rubens Caram [a,*]

[a] University of Campinas (UNICAMP), School of Mechanical Engineering, Campinas, SP 13083-860, Brazil
[b] Welding Engineering, Department of Materials Science and Engineering, The Ohio State University, 1248 Arthur E. Adams Drive, Columbus, OH 43221, USA

HIGHLIGHTS

- Three novel Ti-Nb-Fe-Zr and Ti-Nb-Fe-Sn alloys were empirically developed for biomedical applications.
- Zr and Sn additions reduce the omega-phase formation upon quenching, increasing ductility.
- Ti-19Nb-2.5Fe-10Zr (wt%) water-quenched samples achieved an elastic admissible strength of 1.49.
- After aging, Zr and Sn are equally distributed between the beta-matrix and alpha-precipitates.
- Aged Ti-19Nb-2.5Fe-6Sn (wt%) samples presented a yield strength of 1271 MPa.

GRAPHICAL ABSTRACT

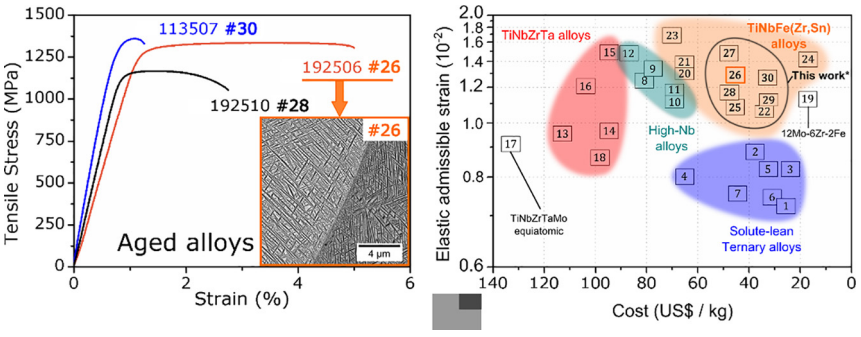

ARTICLE INFO

Article history:
Received 4 June 2018
Received in revised form 11 October 2018
Accepted 26 October 2018
Available online 27 October 2018

Keywords:
Titanium alloys
Phase transformations
Mechanical properties
Materials selection
Biomaterials
Gum metals

ABSTRACT

An open challenge on structural biomaterials is to obtain low-cost Ti-alloys with high elastic admissible strength (the ratio of yield strength to modulus). To reach this goal, we designed and characterized three quaternary alloys from the Ti-Nb-Fe system with additions of Zr and Sn. The samples were solution-treated and tested under two conditions: water-quenched and aged at 450 °C. Microstructures were analyzed with aid of scanning and transmission electron microscopy. Tensile tests performed at room-temperature confirmed a remarkable yield strength of 1271 MPa with an elastic modulus close to 90 GPa among aged Ti-19Nb-2.5Fe-6Sn (wt%) samples. Solution-treated Ti-19Nb-2.5Fe-10Zr samples presented a good combination of yield-strength and elastic modulus (1027 MPa and 69 GPa, respectively), displaying an elastic admissible strength close to 1.5. Although Zr and Sn are equally distributed between matrix and precipitates, the diffusion of Nb and Fe seem to be inhibited by the presence of Sn. As a result, Sn allows higher yield-strengths and more refined secondary α-phase, while Zr has a stronger effect on reducing the elastic modulus. In the end, a materials selection chart is presented to help designers to select materials for orthopedic implants considering the elastic admissible strain and cost as major guidelines.

© 2018 Published by Elsevier Ltd.

1. Introduction

Beta-type titanium (Ti) alloys are designed to retain a metastable β-phase (bcc) when quenched from the β-phase field to room temperature. The pursuit of optimal beta-type Ti alloys for long-term

* Corresponding author.
E-mail address: caram@fem.unicamp.br (R. Caram).
[1] M.R. Dal Bó and C.A.F. Salvador equally contributed to this article.

https://doi.org/10.1016/j.matdes.2018.10.040
0264-1275/© 2018 Published by Elsevier Ltd.

implantation in the human body took off in the 80s [1–3], but it was only in 2003 that technical details of the alloy known as "gum metal" - Ti-23Nb-2Zr-0.7Ta-1.2O (mol %) - were first published by Saito et al. [4]. With a reduction in stiffness, a nonlinear elastic deformation during cold-working, high-strength, low elastic modulus and a good biocompatibility, gum metal and related alloys ascended into the orthopedic implants industry to satisfy the technological needs of hip and knee replacements, and nowadays are considered as benchmark materials in the field [5,6].

At first, it was thought that the outstanding mechanical properties of gum metal were associated with three specific "magic-numbers": the electron/atom ratio, the bond-order (Bo) and the *d*-electron orbital energy level (Md), based on a materials design theory from the 90s [4,7,8]. Despite some useful insights derived from this theory - e.g. that the presence of O, Al, Sn and Zr alter the stability of β and ω phases upon water-quenching (WQ) - the presumption of such "magic numbers" has already been discredited. Talling et al. substituted Nb with V to produce an alloy with the exact same electronic parameters of the original composition, however, the V-based alloy showed a contrasting deformation behavior comparing to the base one [9].

Other early assumption, that gum metals could bear plastic deformation without dislocation glide, was also debunked [10]. Studies on their deformation mechanism identified many concurrent deformation mechanisms such as deformation-induced α″-phase, stress-induced ω-phase, twinning and dislocation glide during strain [11–14]. More recently, Zhang and co-authors identified an α-ω planar complexion induced by the α″ formation after subjecting an oxygen-free gum metal to heating and cooling cycles. The reported complexion contains in its configuration most of the microstructural features observed before, during deformation [15]. After all, it is now clear that the crucial points to be addressed when designing new gum-type alloys are not the magic numbers themselves, but making the alloy vulnerable to SIM (stress-induced martensite formation) while partially suppressing the transformation with proper alloying elements [9,16] – for example, by controlling the oxygen content in the material [17]. In this work, we employed a combination of Nb and Fe to achieve this goal. With the suppression of the orthorhombic martensite (α″-phase) by Fe additions [18,19], Fe simultaneously creates barriers to dislocation motion, increasing strength via solid solution, and allows a reduction in the Nb content (since Fe is a strong beta-stabilizer) – thus reducing cost.

Despite all the evidence of the maturity of TiNbZrTa-based (TNZT) gum metals in the biomedical industry, a remarkable number of studies investigating new formulations of gum-type alloys have been published during the last decade. They reveal the potential of Ti-Nb-Fe-based (TNF) alloys for biomedical applications [20–27]. In a way, researchers have been trying to reduce the cost of the alloys by substituting Nb, Ta, and Mo, which are relatively expensive, with elements abundant all over the world, such as Fe, Sn and Mn [6,28]. Following this trend, we empirically designed cost-effective gum metals from the Ti-Nb-Fe-Zr and Ti-Nb-Fe-Sn systems. Microstructures and mechanical properties were analyzed in two conditions: solution-treated followed by WQ and an arbitrary aging condition. Considering orthopedic applications, the parameter defined as elastic admissible strain (i.e. the ratio of yield strength to elastic modulus) must be maximized in order to avoid failures due to fatigue, associated with low strength, or the activation of the stress-shielding effect, associated with a high elastic modulus [6,29]. Thus, mechanical properties of the experimental alloys were probed and ultimately displayed in an Ashby map that includes a compilation of 24 recently-developed compositions from the literature to guide the selection of biomedical Ti-alloys with optimal mechanical properties and relatively low cost.

2. Experimental

Three experimental alloys with compositions of Ti-19Nb-2.5Fe-10Zr, Ti-19Nb-2.5Fe-6Sn and Ti-11Nb-3.5Fe-7Zr (wt%) were melted under controlled atmosphere (Ar 99.99%) in electric-arc furnace with a refrigerated Cu-crucible. In the illustrations and tables of this paper, the alloys are referred to as 192510, 192506 and 113507, respectively. The ingots weighted 70 g. Precursor elements with high purity (>99.95 wt%) were employed. After solidification, the ingots were homogenized at 1000 °C for 12 h to assure chemical homogeneity. The composition was confirmed by X-ray fluorescence technique (XRF) using a Shimadzu EDX7000 equipment and the interstitial O and N contents were analyzed with a LECO TC400 analyzer (Table 1). Samples were cut using a diamond abrasive saw and cold rolled to 50% of their original thickness. They were then submitted to solution heat-treatment (ST) at 800 °C for 10 min followed by water quenching (WQ). The second group of samples was subjected to solution treatment (ST) followed by an isothermal step-quench at 450 °C instead. The isothermal aging time varied between 30 min and 12 h, depending on the composition. All samples were subjected to metallographic preparation, including 400, 800, and 1500 grit sandpaper followed by 6 h of vibratory polishing with colloidal silica. Kroll's etching solution was used only on samples examined by optical microscopy. Hardness values were obtained from the Vickers test - seven prints in each sample with 1 kgf applied load for 15 s. The equipment used in such measures was a Buehler 2100. Elastic modulus measurements were obtained by pulse-echo ultrasound technique, coupling longitudinal and transversal waves. Samples with 2 mm thickness were analyzed.

Scanning electron microscopy (SEM) was performed using an FEI Inspect F50 and an FEI Apreo system. FIB foils were prepared from the bulk samples using an FEI Helios 600 and analyzed on an FEI Tecnai F20 equipped with energy-dispersive X-ray spectroscopy (EDX). After all, tensile tests were carried out in an MTS 810 tensile testing equipment using cylindrical tensile specimens with a gauge length of 20 mm. The specimens were heated up to 1000 °C for 5 min and then hot-swaged into cylinders before milling to the final shape. An average of 3 specimens was analyzed for each condition.

3. Results and discussion

3.1. Water-quenched samples

In the case of Ti-19Nb-2.5Fe-10Zr, the combined addition of 19Nb, 2.5Fe and 10Zr (wt%) allowed the retention of a full β-phase after ST-WQ. Nb and Fe additions also play an important role in avoiding the formation of α″-phase [22]. For the other two experimental alloys, athermal-ω (ω_{ath}) was detected (Fig. 1). With that, we infer that the ω-suppression capabilities of 6Sn are not the same as 10Zr (wt%). When comparing the ω-phase detected among the experimental alloys with their respective ternary alloys, quaternary additions with either Sn or Zr reduce the volumetric fraction of ω-phase by some content, as expected [30–32]. The same happens even when the alloys have a similar Mo equivalent - for example, comparing Ti-19Nb-2.5Fe from [27] with and without quaternary additions. Furthermore, the addition of 7Zr to Ti-11Nb-3.5Fe (which has a relatively reduced Nb/Fe ratio) did not suppress the ω_{ath} formation upon WQ, even though the combined presence of Fe and Zr can often destabilize ω [33,34].

Tensile tests performed at the ST-WQ condition are presented in Fig. 2. The average grain-size of Ti-19Nb-2.5Fe-10Zr and Ti-19Nb-2.5Fe-6Sn were estimated at around 70 μm, whilst the grains of Ti-11Nb-3.5Fe-7Zr reached 100 μm, on average, corresponding to Fig. 1a–c. Given the three alloys possess grains with a size of the same order of magnitude, this should not be considered as the main factor while making distinctions between their mechanical properties. The similarities of the stress-strain curves of the Ti-19Nb-2.5Fe-6Sn (wt%) and TNZT gum metals are evident. Just after the specimens start yielding, a drop in the resistance is observed and the stress reaches a plateau, which could be linked to stress-induced phase-transformations, such as α′-phase [35], α″-phase [36], stress-induced ω-phase and deformation twins. According to Koli et al. (2015), deformation mechanisms of Ti alloys vary

Table 1
Compositions (XRF) and interstitial contents of the experimental alloys reported in weight percentage (wt%).

Alloy (wt%)	Ti	Nb	Fe	Zr or Sn	O	N
Ti-11Nb-3.5Fe-7Zr	Bal.	10.9 ± 0.1	3.7 ± 0.1	7.1 ± 0.1	0.164 ± 0.004	0.011 ± 0.001
Ti-19Nb-2.5Fe-6Sn	Bal.	18.6 ± 0.5	2.6 ± 0.1	5.8 ± 0.2	0.128 ± 0.004	0.017 ± 0.001
Ti-19Nb-2.5Fe-10Zr	Bal.	18.9 ± 0.1	2.7 ± 0.1	10.1 ± 0.1	0.157 ± 0.001	0.007 ± 0.001

widely, even within a specific range of solute content [37]. Preliminary XRD data collected on the fractured edges of the tensile test specimens after testing indicate that the main deformation mechanism among the experimental alloys might be twinning and dislocation slip since no stress-induced phases were detected (see Fig. 3). Despite these observations, the influence of ω_{ath} and of the grain-size on the stress-induced formation of α″-phase requires further studies [38].

The strain-hardening effect among Ti-Nb-Fe-Sn (TNFS) samples seems negligible. The ductility of Ti-19Nb-2.5Fe-6Sn is slightly superior to TNZT, with an average strain of 31%, while TNZT-O gets to approx. 20% before failure. According to the literature, at this condition, TNZT-O presents a great combination of yield strength and elastic modulus, 976 MPa and 66 GPa, respectively, thus resulting in an elastic admissible strain (EAS) of 1.48 [6]. Despite the relatively low EAS obtained for Ti-19Nb-2.5Fe-6Sn at this condition (1.09), the EAS obtained for Ti-19Nb-2.5Fe-10Zr (wt%), on the opposite, is fairly close to that of TNZT-O - with 1027 MPa of yield strength and 69 GPa of elastic modulus, as can be seen in Table 2. According to Abdel-Hady et al., Zr has a high bond-order (Bo) comparatively to Ti - thus, alloying with Zr implies in a reduction of the elastic modulus of β-Ti [31]. As examples, Ti–35Nb–5Ta–7Zr and Ti-13Nb-13Zr are commercial alloys which have a considerable amount of Zr added and achieve low elastic moduli,

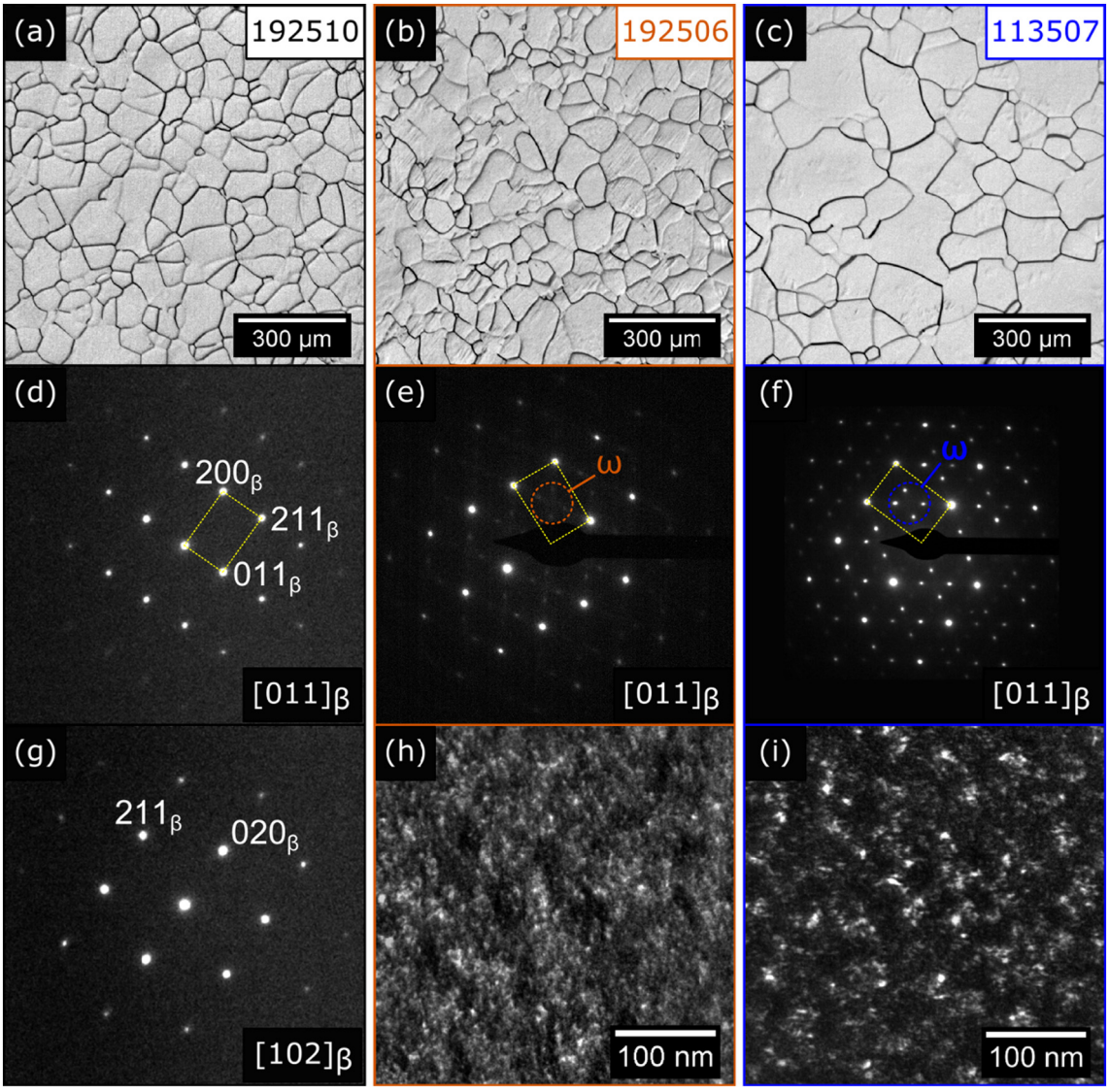

Fig. 1. Optical micrographs of the solution-treated and water-quenched (ST-WQ) quaternary alloys: (a) Ti-19Nb-2.5Fe-10Zr, (b) Ti-19Nb-2.5Fe-6Sn and (c) Ti-11Nb-3.5Fe-7Zr. Selected-area diffraction patterns (SAD, d, e, f) and dark field images showing the athermal omega-phase (h, i) at the same condition. An additional SAD image is presented for Ti-19Nb-2.5Fe-10Zr (g) since it has a full beta-structure at this condition. Ti-19Nb-2.5Fe-6Sn and Ti-11Nb-3.5Fe-7Zr dark-field images are presented in (h) and (i), respectively.

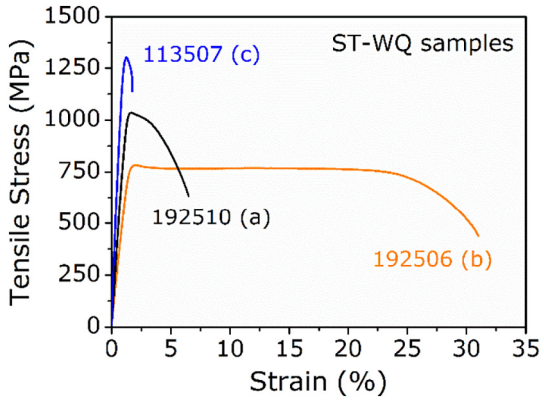

Fig. 2. Stress-strain curves for the experimental alloys at the ST-WQ condition. The plastic deformation does not cause work-hardening among Ti-19Nb-2.5Fe-6Sn (b) samples.

between 55 and 80 GPa, depending on the processing route [6]. As for shape-memory alloys, some authors suggest the optimal Zr/Nb ratio of 0.3 [39]. Whilst Ti-19Nb-2.5Fe-10Zr has a Zr/Nb ratio close to 0.5, it would be worth analyzing its shape-memory behavior at the WQ condition, given the mechanical behavior reported here (Table 3).

To this point, we concluded that the experimental alloys have similar properties to the TNZT system, and quaternary additions benefit the TNF alloys at the ST-WQ condition by increasing the mechanical strength whilst reducing the elastic modulus. As can be seen in the fracture surfaces presented in Fig. 4, all ST-WQ samples showed a relatively ductile behavior, presenting a quasi-cleavage fracture mode [40–42]. The greater proportion of cleavage facets among samples is observed in Ti-11Nb-3.5Fe-7Zr, probably due to the higher ω_{ath} volumetric fraction (Fig. 1) and its elevated Fe content, which is associated with a brittle behavior.

3.2. Isothermally-aged samples

Previous works have shown that Fe largely improves the mechanical strength of TNF alloys due to the reinforcement of the β-phase matrix via solid solution [23,27,43,44]. However, to achieve an even higher strength, a controlled precipitation of alpha (α) through aging heat

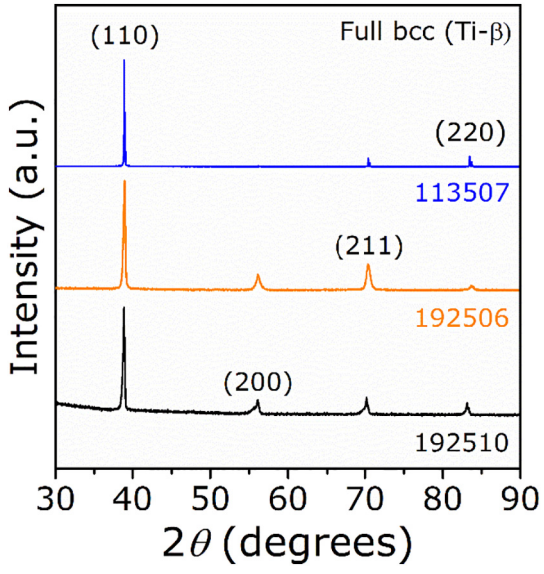

Fig. 3. X-ray diffraction of the fractured edges of the tensile test specimens (after testing) at the ST-WQ condition. Only the β-phase (bcc) was detected.

Table 2
Electronic parameters, hardness and elastic modulus of the experimental alloys. Ternary Ti-11Nb-3.5Fe and Ti-19Nb-2.5Fe were included for comparison.

Alloy	Bo	Md (eV)	e/a	Mo [eq]	Hardness (HV1)	E (GPa)[a]	Ref
1135	2.804	2.399	4.19	11.83	382 ± 3	97 ± 1	[27]
113507	2.817	2.416	4.19	11.83	358 ± 3	88 ± 3	This work
1925	2.820	2.409	4.20	11.57	334 ± 4	90 ± 3	[27]
192506	2.807	2.398	4.21	11.57	260 ± 9	78 ± 1	This work
192510	2.840	2.437	4.21	11.57	267 ± 3	70 ± 1	This work

[a] Obtained with the pulse-echo ultrasound technique.

treatments could be employed [45,46]. Since the size and distribution of α-laths typically vary depending on the aging heat-treatments [47], trials with three different times (30 min, 3 h, and 12 h) were conducted, and we selected the microstructure with the finest and most disperse distribution of α-phase for each alloy to perform the tensile tests. That is - 12 h for the Ti-19Nb-2.5Fe based alloys and 30 min for the Ti-11Nb-3.5Fe-7Zr alloy. The goal was to observe a net increase in the elastic admissible strain after the heat-treatment. Step-quench heat-treatments were selected instead of classical quench-and-aging treatments to avoid the formation of ω-phase at lower temperatures, e.g. while reheating the microstructure [48,49]. The aging temperature of 450 °C was selected based on our previous experiments with Ti-19Nb-2.5Fe ternary alloys [27].

As shown in Fig. 5, an increase in yield strength was observed after aging for all experimental alloys, when compared to the ST condition. Ti-19Nb-2.5Fe-6Sn presented a remarkable increase in yield strength, from 765 MPa to 1261 MPa. Among Zr-based alloys, yield strength was increased by roughly 10%. In other ways, it is known that by strengthening the β matrix through precipitation-hardening, the elastic modulus will inevitably be increased, which is undesirable [3]. The elastic modulus of Ti-19Nb-2.5Fe-10Zr and Ti-19Nb-2.5Fe-6Sn were increased by approximately 30 GPa as part of the heat-treatment performed. These significant changes in the mechanical behavior can be ascribed to microstructural alterations arising from aging, which will be discussed in more detail in the next paragraphs. To some extent, the increase in modulus is also associated with the increase in oxygen content to approx. 0.30 wt% during the hot swaging process, which is a required step in the fabrication of the tensile test specimens (see Supplementary Table 1). Regarding the fracture surfaces, we could identify fewer dimples, compared to the WQ samples, but the typical transgranular fracture mode is still predominant (Fig. 6).

As seen in the scanning electron microscopy (SEM) images presented in Fig. 7, the aging heat-treatment was successful in obtaining fine and disperse α-laths to reinforce the β-matrix for the three experimental alloys. The laths are fairly distributed, acting as an effective barrier to dislocations [47], and we did not observe a massive of α-phase at the grain boundaries, which could impair ductility [40]. With the

Table 3
Compilation of the mechanical properties obtained through tensile tests.

Alloy	Condition	Elastic modulus (GPa)	Yield Strength (MPa)	EAS[a] (%)	Elongation (%)
113507	WQ	90 ± 2	1011 ± 17	1.12	4 ± 1
	Aged	93 ± 2	1184 ± 33	1.27	1 ± 1
192506	WQ	71 ± 2	765 ± 10	1.08	31 ± 5
	Aged	98 ± 3	1261 ± 41	1.29	6 ± 1
192510	WQ	69 ± 1	1027 ± 33	1.49	8 ± 2
	Aged	97 ± 3	1132 ± 18	1.17	3 ± 1

[a] Elastic admissible strain.

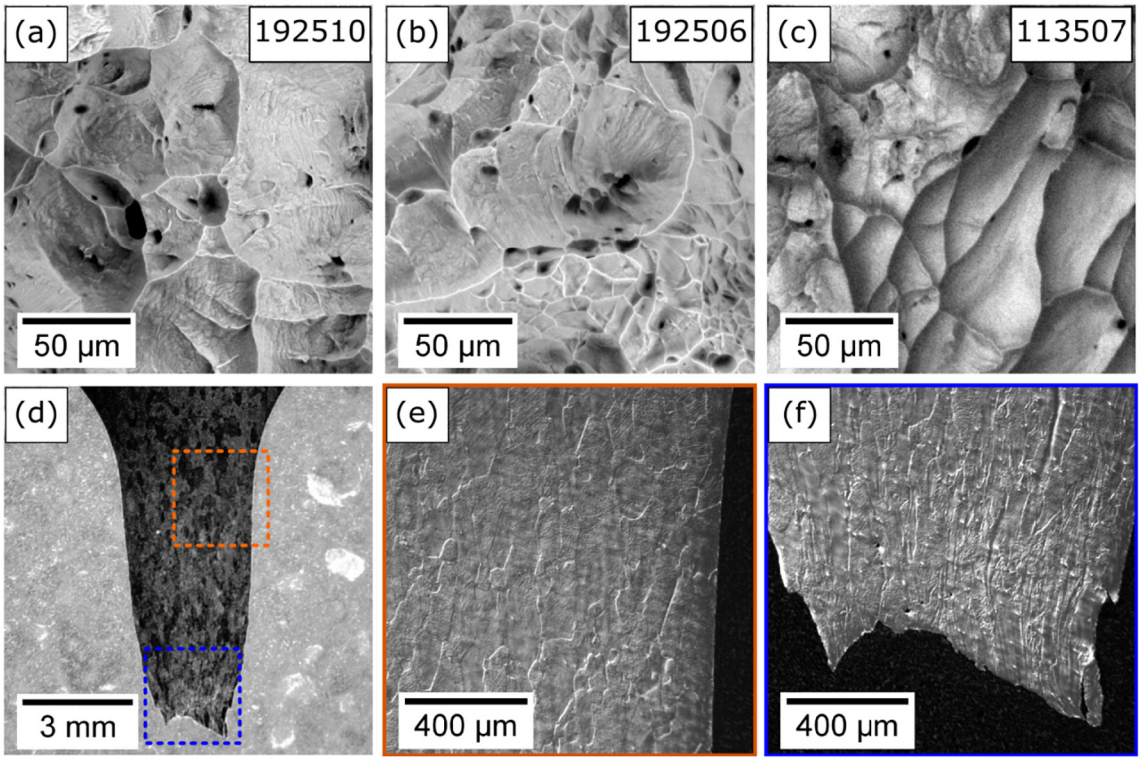

Fig. 4. Fractography of alloys (a) Ti-19Nb-2.5Fe-10Zr (b) Ti-19Nb-2.5Fe-6Sn and (c) Ti-11Nb-3.5Fe-7Zr alloy at the ST-WQ condition. Transversal analysis of the Ti-19Nb-2.5Fe-6Sn showing the increase of martensite laths near the failure (d–f).

assistance of ImageJ2 [50], we estimated the number of α-laths per area in each SEM image displayed in Fig. 7. For Ti-19Nb-2.5Fe-10Zr (Fig. 7b), there are approximately 7 laths/μm^2, while for Ti-19Nb-2.5Fe-6Sn and Ti-11Nb-3.5Fe-7Zr, there are 25 laths/μm^2, corresponding to the average between Fig. 7c and d. The distributions of Ti-19Nb-2.5Fe-6Sn and Ti-11Nb-3.5Fe-7Zr are similar, and both are finer than the Ti-19Nb-2.5Fe-10Zr counterpart. According to Zheng et al., they can be considered super-refined [51]. Finer α-phase distributions usually increase the mechanical strength of Ti-alloys [52], thus, the high strength exhibited by aged Ti-19Nb-2.5Fe-6Sn is certainly related to the regular and restricted growth of α-laths in the selected aging condition. On the other hand, despite its fine α-phase density, the excess of Fe in Ti-11Nb-3.5Fe-7Zr β-matrix may have impaired the alloys ductility, comparing to the Ti-19Nb-2.5Fe based alloys [23].

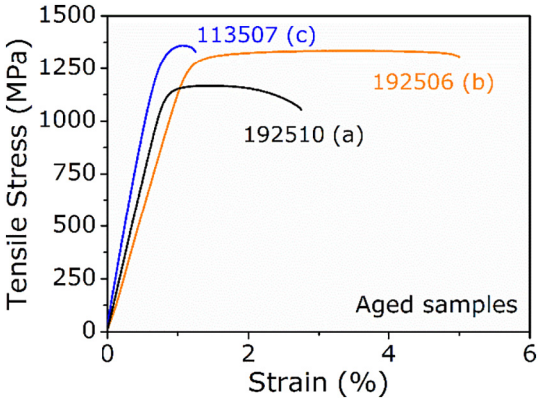

Fig. 5. Stress-strain curves for the heat-treated alloys, (a) Ti-19Nb-2.5Fe-10Zr, (b) Ti-19Nb-2.5Fe-6Sn and (c) Ti-11Nb-3.5Fe-7Zr (wt%).

Regarding the compositional aspects of α-phase formation, the rejection of β-stabilizing Nb and Fe from the α-phase was expected [53]. Additionally, a negligible partitioning of Sn between β-matrix and α-phase laths was observed among Ti-19Nb-2.5Fe-6Sn samples, as shown in Fig. 8. Based on thermodynamic equilibrium assessments via ThermoCalc® (Table 4), the homogeneous distribution of Sn between matrix and precipitates was not expected. Sn should be rejected from the β-phase to the α-laths. However, the opposite trend has been reported while subjecting Ti-Nb-Sn and Ti-Mo-Sn alloys to prolonged aging heat-treatments [54,55], with Sn being slightly rejected to the β-phase, instead. In this respect, it seems the Ti—Sn interactions are not well described via ThermoCalc®, and since the results are controversial, further assessments of the Ti-Fe-Sn system are needed to refine these calculations. The migration of Sn to the β-phase requires time, given Sn low diffusivity in both β and α-phases [56,57]. Thus, 12 h might be not enough time to reach the predicted equilibrium compositions, in this case.

Despite being considered a neutral alloying element, earlier authors suggested that aging Ti-Nb-Zr alloys could induce Zr to migrate to the β-phase matrix, working as a β stabilizer element [58]. However, a Zr partition could not be observed after aging Ti-19Nb-2.5Fe-10Zr for 12 h (Fig. 8b) and Ti-11Nb-3.5Fe-7Zr for 30 min (Fig. 9). ThermoCalc® predictions foresee that Zr should be equally distributed between matrix and precipitates in Ti-19Nb-2.5Fe-10Zr (Table 4), which corroborates with our results. As for Ti-11Nb-3.5Fe-7Zr, Zr should be slightly concentrated at the β-phase. Since we identified the coarsening of the α-precipitates occurring quickly in Ti-11Nb-3.5Fe-7Zr alloy, the heat-treatment time had to be limited to 30 min among these samples to avoid over-aging, and the system also did not have the time to achieve equilibrium compositions. In other ways, the assessment for the Ti-Nb-Fe-Zr system seems accurate.

By comparing Ti-19Nb-2.5Fe-10Zr with Ti-19Nb-2.5Fe-6Sn, we conclude that both Zr and Sn contribute to reducing the elastic modulus comparing to the Ti-Nb-Fe ternary system. The advantage of adding Zr

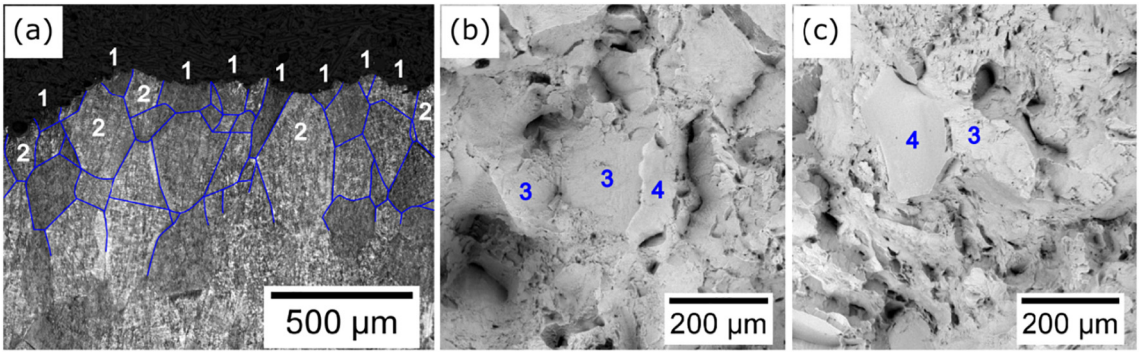

Fig. 6. Transversal (optical) and top-view fractography (a, b) of the Ti-19Nb-2.5Fe-6Sn and top-view (c) of the Ti-11Nb-3.5Fe-7Zr aged samples. Some features are indicated as (1) transgranular fracture, (2) intergranular fracture, (3) mixed fracture and (4) cleavage facets, respectively.

is a stronger effect on reducing the elastic modulus in the ST-WQ condition, while Sn allows higher yield-strengths and more refined α-phase distributions, limiting α-phase coarsening during aging. Therefore, the co-addition of Zr and Sn seems a promising strategy in developing age-hardening gum-type alloys [32,59–61].

3.3. Solute distribution among matrix and precipitates

Now we will discuss the sluggish solute-diffusion observed among the TNFS aged samples, displayed in Fig. 8d. Previous studies showed that nearest-neighbor monovacancy jumps in the ⟨111⟩β direction are responsible for the diffusivity in bcc-structures over a large range of temperatures [62]. According to Neumann et al. (2001), Ti, Zr and Hf-based alloys are vulnerable to lattice instabilities in the ⟨111⟩β direction, which result in a drastic softening of ⟨111⟩ and ⟨110⟩ phonon-modes, that hence cause a decrease of the vacancy-migration energy and thus an enhanced diffusivity [56]. Based on our results, it could be inferred that Sn partially suppresses the lattice instabilities along ⟨111⟩β direction. A consequence of that is the partial suppression of the (111)β collapse (to form ω-phase) observed in the WQ-condition (Fig. 1d–i). On the other hand, since Zr additions also suppressed the ω-phase, this cannot be the main factor influencing the Nb and Fe diffusion in presence of a quaternary element. If that were the case, Ti-Nb-Fe-Zr (TNFZ) and TNFS would display an analogous behavior regarding diffusion (see Figs. 8b, d, 9d). Therefore, the barriers to Nb and Fe diffusions - which are particular to the Ti-Nb-Fe-Sn system - must be related to the presence of Sn atoms in the bcc-solid solution.

Sn has been known as a slow-diffuser in α and β Ti-alloys [56,57,63,64]. Although some authors take account of Sn large metallic radius on its diffusivity, this should not play a decisive role regarding substitutional solutes that migrate via vacancies [56]. The diffusion coefficients of substitutional solutes linearly depend on correlation factors (CFs) - i.e. the correlation between two successive solute-vacancy exchanges. However, in binary alloys, the influence of CFs on Sn diffusion

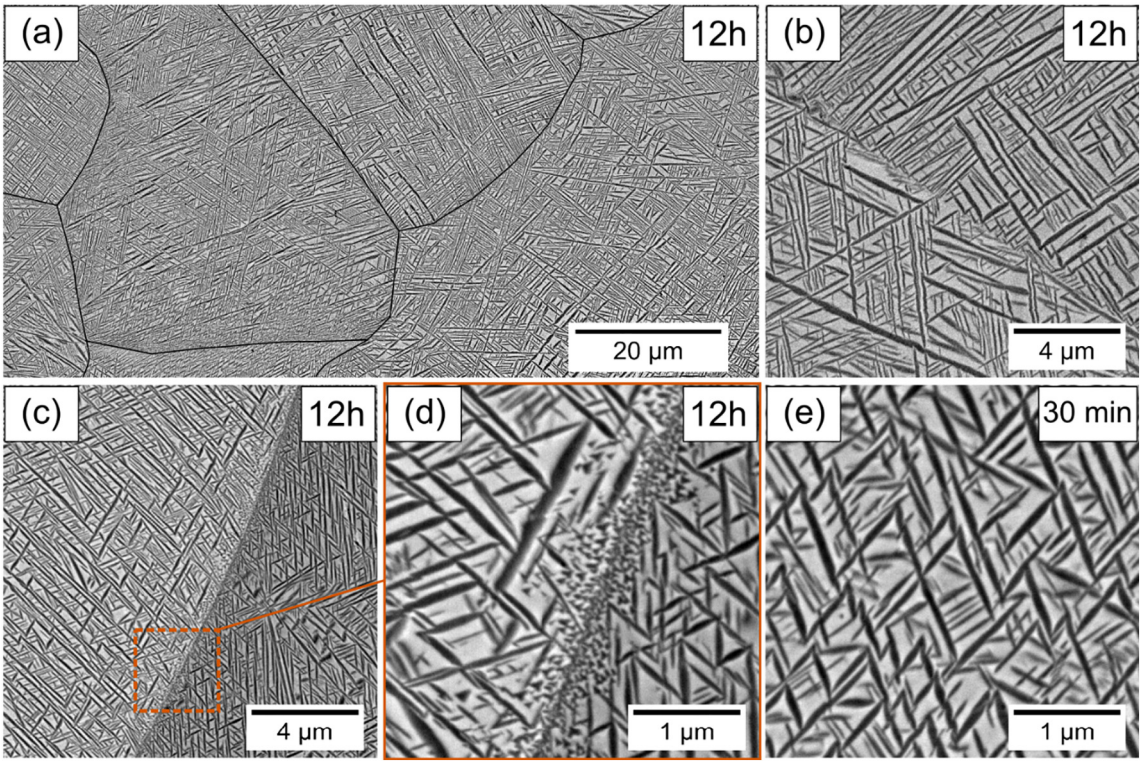

Fig. 7. SEM backscattered electrons (BSE) images of the experimental alloys after aging: (a) low-magnification of Ti-19Nb-2.5Fe-10Zr, grain boundaries were highlighted with coarse black lines; (b) Ti-19Nb-2.5Fe-10Zr, (c, d) Ti-19Nb-2.5Fe-6Sn and (e) Ti-11Nb-3.5Fe-7Zr alloy. The aging time is displayed at the right, upper corner.

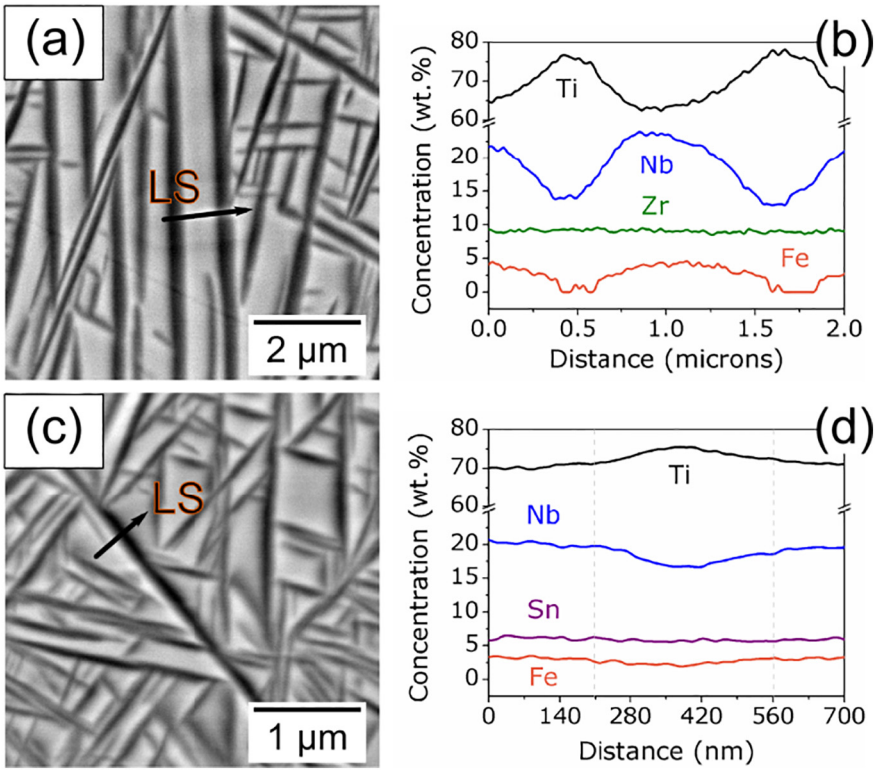

Fig. 8. Line scans performed via scanning electron microscopy (SEM), energy dispersive X-ray spectroscopy (EDX) of Ti-19Nb-2.5Fe-10Zr (a–b) and Ti-19Nb-2.5Fe-6Sn (c–d) aged at 450 °C for 12 h. A marginal partition of both Zr (b) and Sn (d) is observed between matrix and precipitates.

is negligible [63]. As a result, the CFs on Sn impurity-diffusion in β-Ti has been often described by a pure mass-effect [56]. In respect to this point, we can only infer that the CFs in a multi-component system diverge from the binaries correlation factors available in the literature [64]. On top of that, CFs must depend on secondary interactions between Sn and the other alloying elements in this system: Nb and Fe.

According to a recent study with the Ti-Nb-Sn system, small Sn additions create an energetically favorable configuration of Ti—Sn first-neighboring atoms, with a mixed Ti—Nb neighborhood [65]. We believe these Ti—Sn anti-bonding sites may influence the vacancy-migration energy and therefore the solute diffusion in our system. After all, further studies on the solute-vacancy binding energies and on the chemical bonding characteristics of the Ti-Nb-Fe-Sn quaternary system are needed to reach a better understanding of the role of Sn on the mechanisms of diffusion.

3.4. Materials selection and documentation

Materials property charts (Ashby maps) are useful tools for selecting materials for structural parts. They represent, in a concise way, how two properties of interest correlate with each other. Also, by analyzing the position of a given material on the chart, one can promptly have a dimension on how the material will perform compared to other candidates with respect to these properties [66].

Table 4
Equilibrium compositions at 450 °C predicted by ThermoCalc® using TCT1.

Alloy (wt%)	Phases[a]	Composition (wt%)			
		Ti	Nb	Fe	Zr or Sn
Ti-11Nb-3.5Fe-7Zr	β (bcc)	60.3	22.9	8.6	8.2
	α (hcp)	91.0	2.8	<0.01	6.1
Ti-19Nb-2.5Fe-6Sn	β (bcc)	46.1	47.4	6.5	<0.01
	α (hcp)	90.0	1.3	<0.01	9.7
Ti-19Nb-2.5Fe-10Zr	β (bcc)	52.4	32.9	4.7	10.0
	α (hcp)	86.9	3.1	<0.01	10.0

[a] Only disordered BCCs were included in the calculation.

With Fig. 10, we provide a detailed comparison of the alloys proposed in this study and 24 other compositions taken from the literature. Individual points in the graph are displayed as numbers, each one associated to an alloy listed in the Supplementary Table 2. As properties of interest for the map, we selected the elastic admissible strain, a well-developed performance index to structural biomaterials, and the alloy cost, which was estimated based on the cost-per-weight of the base-metals traded on the London Metal Exchange (2016 first quarter), available here [67], and its relative proportion in each alloy.

From left to right, upper on the chart, we can spot #15 (TNZT-O) and #12 (Ti-42Nb-O). As expected, TNZT and related alloys (in red) perform well in terms of elastic admissible strain, however, their cost is elevated due to the high percentage of Nb, Ta, and Zr in their composition - that is why they are displayed far left on the chart. Ternary alloys as the ones reported by Biesiekierski et al. (Ti-34Nb-25Zr) and Bahl et al. (Ti-32Nb-2Sn), #9 and #10, respectively, have a relatively high elastic admissible strain, but their high-Nb content makes them a bit expensive (centered on the chart).

On the lower part of the chart, in violet, we expose the limitations of solute-lean ternary alloys such as (#1) Ti-6Al-4V, (#2) Ti-13Nb-13Zr and other alloys from the TNF system (#4–#7). They barely achieve an elastic admissible strain of 1.0. In a recent study, we compared six novel compositions derived from the Ti-Nb-Fe (TNF) system to establish the dependence of the elastic modulus on the Nb/Fe atomic ratio [27]. Among samples submitted to solution-treatment followed by water-quenching, the elastic modulus is always higher than 80 GPa due to the presence of ω_{ath} phase [27,46,68], which also limited their cold-workability. On the other hand, Ti-6Al-4V has a good yield strength, but its elastic modulus is higher than 100 GPa, which is undesirable considering the activation of stress-shielding [29]. Despite the low-cost associated with these alloys, they are deficient in terms of either yield strength or elastic modulus.

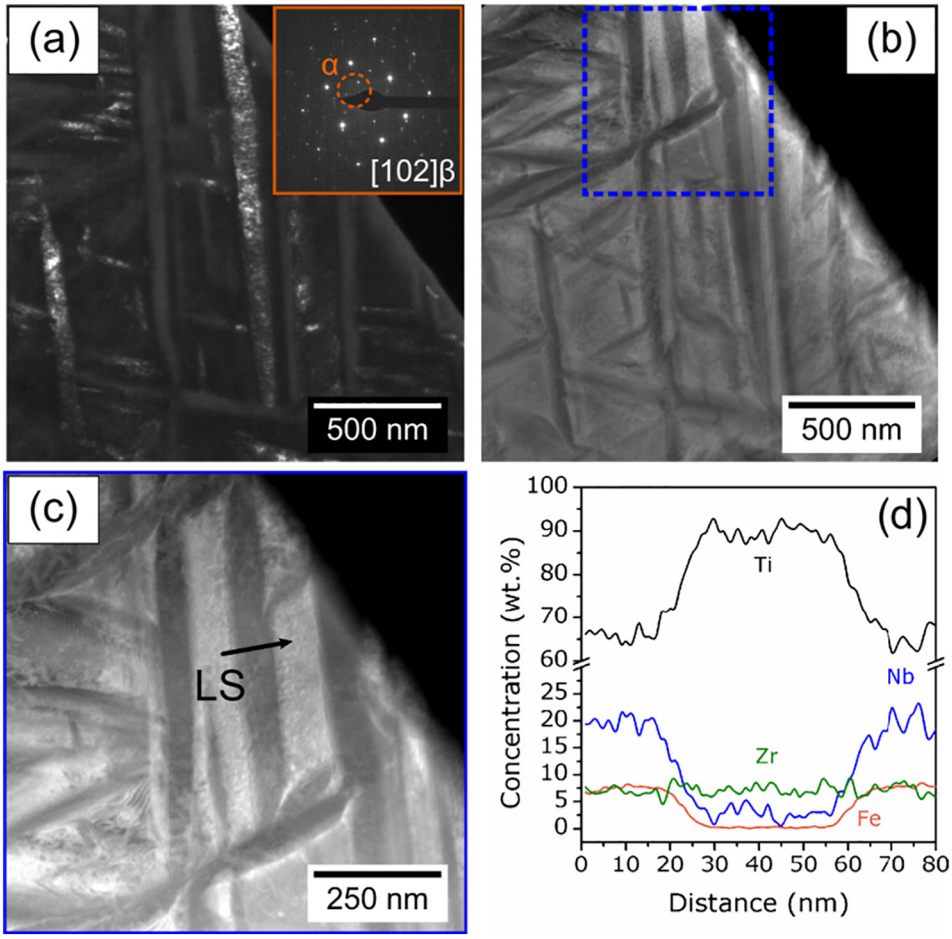

Fig. 9. TEM-images of Ti-11Nb-3.5Fe-7Zr aged at 450 °C for 30 min: (a) dark-field showing the alpha-precipitates through the [102]β zone axis, (b) HAADF image of the same region, (c) HAADF showing the region analyzed via EDX and finally (d) the compositional profile of the marked α-lath.

Through a combined analysis, the best candidates with a trade-off between elastic admissible strain and cost are displayed in the first quadrant of Fig. 10. They are: #24 (Ti-5Fe-3Nb-3Zr), #19 (Ti-12Mo-6Zr-2Fe) and numbers #26, #27 and #30, designed in this study. These numbers refer to Ti-19Nb-2.5Fe-6Sn at the aged condition, Ti-19Nb-2.5Fe-10Zr at the ST-WQ condition, Ti-11Nb-3.5Fe-7Zr at the aged condition, respectively. We must highlight the position of #27 (Ti-19Nb-2.5Fe-10Zr) which presented a remarkable elastic admissible strain of 1.49. Also upper on the chart, but with a slightly higher cost, are the remaining alloys from the TNZF system: #23 (Ti-32Nb-6Zr-1.5Fe, Nocivin et al. [26]), #20 and #21 (Ti-28Nb13Zr-0.5Fe, Cui et al. [20]). It may be emphasized that we considered the price of commercially pure Nb (99.9%) to compose the price of all TNZF based alloys. Nevertheless, the expense could be partially reduced by using Nb—Fe master alloys (66%Nb, 33%Fe) instead, since these alloys have both Nb and Fe in their composition. Master alloys are commodities of the steel industry, and their costs are far inferior to the vacuum-grade Nb counterpart. As an exception in the first quadrant, Ti-12Mo-6Zr-2Fe alloy (ASTM F1813, [69]) shows that Ti—Mo based alloys can also perform well within the selected criteria. However, Ti—Nb based alloys are superior in respect of wear behavior. According to the literature, Nb allows a quick re-passivation at the surface level, preventing any premature failure due to combined corrosion-wear mechanisms [3].

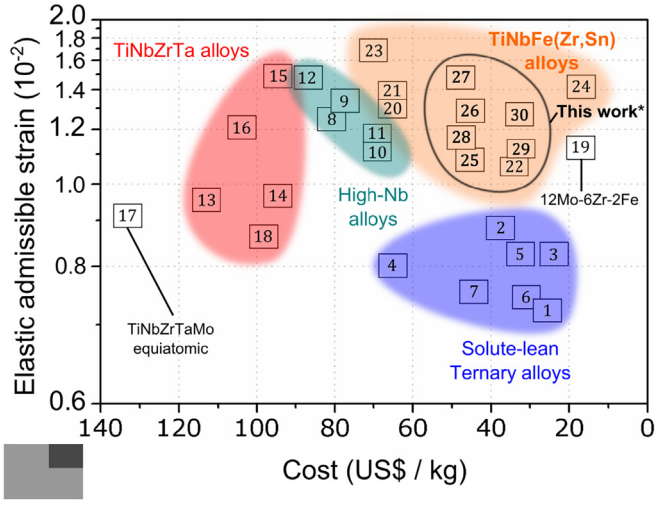

Fig. 10. Ashby map displaying some biomedical alloys from the literature and the ones analyzed in this study. The 30 individual points displayed in the graph can be found, with the respective references, on Table S2 (Supplementary information).

It is worth reminding that in Fig. 10, alloys subjected to ST-WQ and to intricate heat-treatments are compared all at once, thus, their microstructure is varied. For more information, please check Supplementary Table 2. Also, with the precipitation of α-phase during aging-heat treatments, both yield strength and elastic modulus are increased [49,70], and a specific EAS can be found for either condition, depending on the alloy.

4. Conclusions

With the exposed limitations of the Ti-Nb-Fe ternary system in mind [27], the results of this study showed that the addition of ω suppressor

elements such as Zr and Sn to Ti-Nb-Fe alloys are important to obtain low-modulus, low-cost quaternary alloys, with good cold-formability. Therefore, these additions are always beneficial to the Ti-Nb-Fe alloys, drastically improving the EAS (elastic admissible strain) compared to the ternary alloys. Alongside with improvements such as proper cold working, grain refinement, and oxygen addition, we believe the TNFZ and TNFS alloys reported here can easily achieve 1.4 GPa of yield strength while maintaining a low elastic modulus, near 70 GPa. Ti-19Nb-2.5Fe-10Zr is best represented at the ST-WQ condition, while Ti-19Nb-2.5Fe-6Sn was presented as a viable age-hardening alloy. Also, the alloys developed in this study are cost-effective, with an average price lower than 40 US$/kg, while the conventional TNZT gum metals cost nearly 100 US$/kg.

Supplementary data to this article can be found online at https://doi.org/10.1016/j.matdes.2018.10.040.

Acknowledgments

Funding: This work was supported by FAPESP (São Paulo State Research Foundation, grants numbers 2014/24449-0, 2016/22714-3 and 2016/24693-3) and CNPq (National Council for Scientific and Technological Development). The authors gratefully acknowledge Prof. Hamish Fraser for the use of experimental facilities at the Center for Electron Microscopy and Analysis (CEMAS), at the Ohio State University, USA, and thank CBMM Co. for the Nb supply.

The raw/processed data required to reproduce these findings cannot be shared at this time as the data also forms part of an ongoing study. Data will be made available upon request.

References

[1] M. Semlitsch, H.G. Willert, Properties of implant alloys for artificial hip joints, Med. Biol. Eng. Comput. 18 (1980) 511–520, https://doi.org/10.1007/BF02443329.
[2] M. Semlitsch, Titanium alloys for hip joint replacements, Clin. Mater. 2 (1987) 1–13, https://doi.org/10.1016/0267-6605(87)90015-1.
[3] M. Geetha, A.K. Singh, R. Asokamani, A.K. Gogia, Ti based biomaterials, the ultimate choice for orthopaedic implants – a review, Prog. Mater. Sci. 54 (2009) 397–425, https://doi.org/10.1016/j.pmatsci.2008.06.004.
[4] T. Saito, T. Furuta, J.-H. Hwang, S. Kuramoto, K. Nishino, N. Suzuki, R. Chen, A. Yamada, K. Ito, Y. Seno, T. Nonaka, H. Ikehata, N. Nagasako, C. Iwamoto, Y. Ikuhara, T. Sakuma, Multifunctional alloys obtained via a dislocation-free plastic deformation mechanism, Science 300 (2003) 464–467, https://doi.org/10.1126/science.1081957.
[5] M. Niinomi, M. Nakai, Titanium-based biomaterials for preventing stress shielding between implant devices and bone, Int. J. Biomater. 2011 (2011), 836587. https://doi.org/10.1155/2011/836587.
[6] M. Abdel-Hady Gepreel, M. Niinomi, M.A. Gepreel, M. Niinomi, Biocompatibility of Ti-alloys for long-term implantation, J. Mech. Behav. Biomed. Mater. 20 (2013) 407–415, https://doi.org/10.1016/j.jmbbm.2012.11.014.
[7] K.K.M. Morinaga, M. Kato, T. Kamimura, M. Fukumoto, I. Harada, Theoretical Design of β-type Titanium Alloys, TMS, Warrendale, PA, 1992 276–283.
[8] D. Kuroda, M. Niinomi, M. Morinaga, Y. Kato, T. Yashiro, Design and mechanical properties of new beta type titanium alloys for implant materials, Mater. Sci. Eng. A A243 (1998) 244–249, https://doi.org/10.1016/S0921-5093(97)00808-3.
[9] R.J. Talling, R.J. Dashwood, M. Jackson, D. Dye, Compositional variability in gum metal, Scr. Mater. 60 (2009) 1000–1003, https://doi.org/10.1016/j.scriptamat.2009.02.044.
[10] E. Plancher, C.C. Tasan, S. Sandloebes, D. Raabe, On dislocation involvement in Ti–Nb gum metal plasticity, Scr. Mater. 68 (2013) 805–808, https://doi.org/10.1016/j.scriptamat.2013.01.034.
[11] R. Talling, R. Dashwood, M. Jackson, S. Kuramoto, D. Dye, Determination of (C11-C12C11-C12) in Ti–36Nb–2Ta–3Zr–0.3O (wt.%) (gum metal), Scr. Mater. 59 (2008) 669–672, https://doi.org/10.1016/j.scriptamat.2008.05.022.
[12] R.J. Talling, R.J. Dashwood, M. Jackson, D. Dye, On the mechanism of superelasticity in gum metal, Acta Mater. 57 (2009) 1188–1198, https://doi.org/10.1016/j.actamat.2008.11.013.
[13] E.A. Withey, A.M. Minor, D.C. Chrzan, J.W. Morris Jr, S. Kuramoto, The deformation of gum metal through in situ compression of nanopillars, Acta Mater. 58 (2010) 2652–2665, https://doi.org/10.1016/j.actamat.2009.12.052.
[14] M. Besse, P. Castany, T. Gloriant, Mechanisms of deformation in gum metal TNTZ-O and TNTZ titanium alloys: a comparative study on the oxygen influence, Acta Mater. 59 (2011) 5982–5988, https://doi.org/10.1016/j.actamat.2011.06.006.
[15] J. Zhang, C.C. Tasan, M.J. Lai, A.-C. Dippel, D. Raabe, Complexion-mediated martensitic phase transformation in titanium, Nat. Commun. 8 (2017), 14210. https://doi.org/10.1038/ncomms14210.
[16] J.Y. Zhang, J.S. Li, G.F. Chen, L. Liu, Z. Chen, Q.K. Meng, B.L. Shen, F. Sun, F. Prima, Fabrication and characterization of a novel β metastable Ti-Mo-Zr alloy with large ductility and improved yield strength, Mater. Charact. 139 (2018) 421–427, https://doi.org/10.1016/j.matchar.2018.03.031.
[17] E.G. Obbard, Y.L. Hao, R.J. Talling, S.J. Li, Y.W. Zhang, D. Dye, R. Yang, The effect of oxygen on α″ martensite and superelasticity in Ti–24Nb–4Zr–8Sn, Acta Mater. 59 (2011) 112–125, https://doi.org/10.1016/j.actamat.2010.09.015.
[18] S. Cai, J.E. Schaffer, Y. Ren, Stress-induced phase transformation and room temperature aging in Ti-Nb-Fe alloys, Mater. Sci. Eng. A 680 (2017) 13–20, https://doi.org/10.1016/j.msea.2016.10.060.
[19] S. Ehtemam-Haghighi, Y. Liu, G. Cao, L.-C. Zhang, Influence of Nb on the β → α″ martensitic phase transformation and properties of the newly designed Ti–Fe–Nb alloys, Mater. Sci. Eng. C 60 (2016) 503–510, https://doi.org/10.1016/j.msec.2015.11.072.
[20] W.F. Cui, A.H. Guo, Microstructures and properties of biomedical TiNbZrFe β-titanium alloy under aging conditions, Mater. Sci. Eng. A 527 (2009) 258–262, https://doi.org/10.1016/j.msea.2009.08.057.
[21] Y. Xu, Y. Xiao, D. Yi, H. Liu, L. Wu, J. Wen, Corrosion behavior of Ti–Nb–Ta–Zr–Fe alloy for biomedical applications in Ringer's solution, Trans. Nonferrous Metals Soc. China 25 (2015) 2556–2563, https://doi.org/10.1016/S1003-6326(15)63875-4.
[22] S.E. Haghighi, H.B. Lu, G.Y. Jian, G.H. Cao, D. Habibi, L.C. Zhang, Effect of α″ martensite on the microstructure and mechanical properties of beta-type Ti–Fe–Ta alloys, Mater. Des. 76 (2015) 47–54, https://doi.org/10.1016/j.matdes.2015.03.028.
[23] S. Ehtemam-Haghighi, Y. Liu, G. Cao, L.-C. Zhang, Phase transition, microstructural evolution and mechanical properties of Ti-Nb-Fe alloys induced by Fe addition, Mater. Des. 97 (2016) 279–286, https://doi.org/10.1016/j.matdes.2016.02.094.
[24] A. Biesiekierski, J. Lin, Y. Li, D. Ping, Y. Yamabe-Mitarai, C. Wen, Investigations into Ti–(Nb,Ta)–Fe alloys for biomedical applications, Acta Biomater. 32 (2016) 336–347, https://doi.org/10.1016/j.actbio.2015.12.010.
[25] C. Xiong, P. Xue, F. Zhang, Y. Li, Phase transformations and microstructural evolution in Ti-19.5Zr-10Nb-0.5Fe shape memory alloys, Mater. Charact. 133 (2017) 156–164, https://doi.org/10.1016/j.matchar.2017.09.033.
[26] A. Nocivin, I. Cinca, D. Raducanu, V.D. Cojocaru, I.A. Popovici, Mechanical properties of a gum-type Ti–Nb–Zr–Fe–O alloy, Int. J. Miner. Metall. Mater. 24 (2017) 909–917, https://doi.org/10.1007/s12613-017-1477-3.
[27] C.A.F. Salvador, M.R. Dal Bó, F.H. Costa, M.O. Taipina, E.S.N. Lopes, R. Caram, Solute lean Ti-Nb-Fe alloys: an exploratory study, J. Mech. Behav. Biomed. Mater. 65 (2017) 761–769, https://doi.org/10.1016/j.jmbbm.2016.09.024.
[28] P.F. Santos, M. Niinomi, K. Cho, M. Nakai, H. Liu, N. Ohtsu, M. Hirano, M. Ikeda, T. Narushima, Microstructures, mechanical properties and cytotoxicity of low cost beta Ti-Mn alloys for biomedical applications, Acta Biomater. 26 (2015) 366–376, https://doi.org/10.1016/j.actbio.2015.08.015.
[29] M. Long, H.J. Rack, Titanium alloys in total joint replacement–a materials science perspective, Biomaterials 19 (1998) 1621–1639http://www.ncbi.nlm.nih.gov/pubmed/9839998.
[30] M. Geetha, A.K. Singh, A.K. Gogia, R. Asokamani, Effect of thermomechanical processing on evolution of various phases in Ti–Nb–Zr alloys, J. Alloys Compd. 384 (2004) 131–144, https://doi.org/10.1016/j.jallcom.2004.04.113.
[31] M. Abdel-Hady, K. Hinoshita, M. Morinaga, General approach to phase stability and elastic properties of β-type Ti-alloys using electronic parameters, Scr. Mater. 55 (2006) 477–480, https://doi.org/10.1016/j.scriptamat.2006.04.022.
[32] Y.L. Hao, S.J. Li, S.Y. Sun, R. Yang, Effect of Zr and Sn on Young's modulus and superelasticity of Ti–Nb-based alloys, Mater. Sci. Eng. A 441 (2006) 112–118, https://doi.org/10.1016/j.msea.2006.09.051.
[33] D.J. Lin, J.H.C. Lin, C.P. Ju, Structure and Properties of Ti – 7. 5Mo – xFe Alloys, 23, 2002 1723–1730.
[34] X.H. Min, S. Emura, L. Zhang, K. Tsuzaki, Effect of Fe and Zr additions on ω phase formation in β-type Ti–Mo alloys, Mater. Sci. Eng. A 497 (2008) 74–78, https://doi.org/10.1016/j.msea.2008.06.018.
[35] A. Kilmametov, Y. Ivanisenko, B. Straumal, A.A. Mazilkin, A.S. Gornakova, M.J. Kriegel, O.B. Fabrichnaya, D. Rafaja, H. Hahn, Transformations of α′ martensite in Ti–Fe alloys under high pressure torsion, Scr. Mater. 136 (2017) 46–49, https://doi.org/10.1016/j.scriptamat.2017.04.010.
[36] F. Sun, Y.L. Hao, S. Nowak, T. Gloriant, P. Laheurte, F. Prima, A thermo-mechanical treatment to improve the superelastic performances of biomedical Ti-26Nb and Ti-20Nb-6Zr (at.%) alloys, J. Mech. Behav. Biomed. Mater. 4 (2011) 1864–1872, https://doi.org/10.1016/j.jmbbm.2011.06.003.
[37] R.P. Kolli, W.J. Joost, S. Ankem, Phase stability and stress-induced transformations in Beta titanium alloys, JOM 67 (2015) 1273–1280, https://doi.org/10.1007/s11837-015-1411-y.
[38] T. Grosdidier, Y. Combres, E. Gautier, M.J. Philippe, Effect of microstructure variations on the formation of deformation-induced martensite and associated tensile properties in a β metastable Ti alloy, Metall. Mater. Trans. A Phys. Metall. Mater. Sci. 31 (2000) 1095–1106, https://doi.org/10.1007/s11661-000-0105-3.
[39] F. Sun, S. Nowak, T. Gloriant, P. Laheurte, a. Eberhardt, F. Prima, Influence of a short thermal treatment on the superelastic properties of a titanium-based alloy, Scr. Mater. 63 (2010) 1053–1056, https://doi.org/10.1016/j.scriptamat.2010.07.042.
[40] L.C. Campanelli, P.S.C.P. da Silva, C. Bolfarini, High cycle fatigue and fracture behavior of Ti-5Al-5Mo-5V-3Cr alloy with BASCA and double aging treatments, Mater. Sci. Eng. A 658 (2016) 203–209, https://doi.org/10.1016/j.msea.2016.02.004.
[41] V.C. Opini, C.A.F. Salvador, K.N. Campo, E.S.N. Lopes, R.R. Chaves, R. Caram, α phase precipitation and mechanical properties of Nb-modified Ti-5553 alloy, Mater. Sci. Eng. A 670 (2016) 112–121, https://doi.org/10.1016/j.msea.2016.06.001.
[42] F.H. da Costa, C.A.F. Salvador, M.G. de Mello, R. Caram, Alpha phase precipitation in Ti-30Nb-1Fe alloys – phase transformations in continuous heating and aging heat

treatments, Mater. Sci. Eng. A 677 (2016)https://doi.org/10.1016/j.msea.2016.09.023.
[43] J.M. Chaves, O. Florêncio, P.S. Silva, P.W.B. Marques, C.R.M. Afonso, Influence of phase transformations on dynamical elastic modulus and anelasticity of beta Ti–Nb–Fe alloys for biomedical applications, J. Mech. Behav. Biomed. Mater. 46 (2015) 184–196, https://doi.org/10.1016/j.jmbbm.2015.02.030.
[44] É.S.N. Lopes, C.A.F. Salvador, D.R. Andrade, A. Cremasco, K.N. Campo, R. Caram, Microstructure, mechanical properties, and electrochemical behavior of Ti-Nb-Fe alloys applied as biomaterials, Metall. Mater. Trans. A 47 (2016) 3213–3226, https://doi.org/10.1007/s11661-016-3411-0.
[45] S. Bahl, A.S. Krishnamurthy, S. Suwas, K. Chatterjee, Controlled nanoscale precipitation to enhance the mechanical and biological performances of a metastable β Ti-Nb-Sn alloy for orthopedic applications, Mater. Des. 126 (2017) 226–237, https://doi.org/10.1016/j.matdes.2017.04.014.
[46] F.H. da Costa, C.A.F. Salvador, M.G. de Mello, R. Caram, Alpha phase precipitation in Ti-30Nb-1Fe alloys – phase transformations in continuous heating and aging heat treatments, Mater. Sci. Eng. A 677 (2016) 222–229, https://doi.org/10.1016/j.msea.2016.09.023.
[47] D. Banerjee, J.C. Williams, Perspectives on titanium science and technology, Acta Mater. 61 (2013) 844–879, https://doi.org/10.1016/j.actamat.2012.10.043.
[48] S. Kobayashi, R. Ohshima, K. Nakai, T. Sakamoto, Effect of quenching and reheating on isothermal phase transformation in Ti-15Nb-10Zr alloy, Mater. Sci. Forum 638–642 (2010) 582–587, https://doi.org/10.4028/www.scientific.net/MSF.638-642.582.
[49] C.A.F. Salvador, V.C. Opini, E.S.N. Lopes, R. Caram, Microstructure evolution of Ti–30Nb–(4Sn) alloys during classical and step-quench aging heat treatments, Mater. Sci. Technol. 33 (2017) 400–407, https://doi.org/10.1080/02670836.2016.1216030.
[50] C.T. Rueden, J. Schindelin, M.C. Hiner, B.E. Dezonia, A.E. Walter, E.T. Arena, K.W. Eliceiri, ImageJ2: ImageJ for the next generation of scientific image data, BMC Bioinf. 18 (2017), 529. https://doi.org/10.1186/s12859-017-1934-z.
[51] Y. Zheng, R.E.A. Williams, D. Wang, R. Shi, S. Nag, P. Kami, J.M. Sosa, R. Banerjee, Y. Wang, H.L. Fraser, Role of ω phase in the formation of extremely refined intragranular α precipitates in metastable β-titanium alloys, Acta Mater. 103 (2016) 850–858, https://doi.org/10.1016/j.actamat.2015.11.020.
[52] M.-Y. Seok, Y. Zhao, J.-A. Lee, R.M. Mohamed, L.M. Al-Harbi, M.S. Al-Ghamdi, G. Singh, U. Ramamurty, J. Jang, On the contributions of different micromechanisms for enhancement in the strength of TI–6Al–4V alloy upon B addition: a nanomechanical analysis, Mater. Sci. Eng. A 649 (2016) 123–127, https://doi.org/10.1016/j.msea.2015.09.103.
[53] C.A.F. Salvador, E.S.N. Lopes, J. Bettini, R. Caram, Formation of alpha phase via pseudospinodal decomposition in Ti-Nb-Fe based alloys, Mater. Lett. 189 (2017) 201–205, https://doi.org/10.1016/j.matlet.2016.11.097.
[54] M.G. de Mello, C.A.F. Salvador, A. Cremasco, R. Caram, The effect of Sn addition on phase stability and phase evolution during aging heat treatment in Ti–Mo alloys employed as biomaterials, Mater. Charact. 110 (2015) 5–13, https://doi.org/10.1016/j.matchar.2015.10.005.
[55] C.A.F. Salvador, E.S.N. Lopes, C.A. Ospina, R. Caram, Orthorhombic martensite formation upon aging in a Ti-30Nb-4Sn alloy, Mater. Chem. Phys. 183 (2016) 238–246, https://doi.org/10.1016/j.matchemphys.2016.08.023.
[56] G. Neumann, V. To, C. Tuijn, On the impurity diffusion in beta-Ti, Phys. B 296 (2001) 334–341.
[57] R.A. Perez, H. Nakajima, F. Dyment, Diffusion in alpha-Ti and Zr, Mater. Trans. 44 (2003) 2–13.
[58] M. Abdel-Hady, H. Fuwa, K. Hinoshita, H. Kimura, Y. Shinzato, M. Morinaga, Phase stability change with Zr content in β-type Ti–Nb alloys, Scr. Mater. 57 (2007) 1000–1003, https://doi.org/10.1016/j.scriptamat.2007.08.003.
[59] Y.L. Hao, S.J. Li, S.Y. Sun, C.Y. Zheng, R. Yang, Elastic deformation behaviour of Ti–24Nb–4Zr–7.9Sn for biomedical applications, Acta Biomater. 3 (2007) 277–286, https://doi.org/10.1016/j.actbio.2006.11.002.
[60] B. Jiang, Q. Wang, D. Wen, F. Xu, G. Chen, C. Dong, L. Sun, P.K. Liaw, Effects of Nb and Zr on structural stabilities of Ti-Mo-Sn-based alloys with low modulus, Mater. Sci. Eng. A 687 (2017) 1–7, https://doi.org/10.1016/j.msea.2017.01.047.
[61] M.F. Ijaz, H.Y. Kim, H. Hosoda, S. Miyazaki, Superelastic properties of biomedical (Ti-Zr)-Mo-Sn alloys, Mater. Sci. Eng. C 48 (2015) 11–20, https://doi.org/10.1016/j.msec.2014.11.010.
[62] C. Herzig, U. Köhler, S.V. Divinski, Tracer diffusion and mechanism of non-Arrhenius diffusion behavior of Zr and Nb in body-centered cubic Zr – Nb alloys Tracer diffusion and mechanism of non-Arrhenius diffusion behavior of Zr and Nb in body-centered cubic Zr – Nb alloys, J. Appl. Phys. 85 (1999) 8119–8130, https://doi.org/10.1063/1.370650.
[63] X.J. Liu, Z.K. Liu, A first-principles study of the diffusion coefficients of alloying elements in dilute alpha-Ti alloys, PCCP 18 (2016) 16870–16881, https://doi.org/10.1039/C6CP01899H.
[64] J.L. Wang, L.B. Liu, B.Y. Tuo, W.M. Bai, X. Wang, X. Li, X.P. Hu, Computational Study of Mobilities and Diffusion in Ti-Sn Alloy, 36, 2015 248–253, https://doi.org/10.1007/s11669-015-0377-3.
[65] J.J. Gutiérrez-Moreno, Y. Guo, K. Georgarakis, A.R. Yavari, G.A. Evangelakis, C.E. Lekka, The role of Sn doping in the β-type Ti – 25 at % Nb alloys: experiment and ab initio calculations the role of Sn doping in the b -type Ti – 25 at % Nb alloys: experiment and ab initio calculations, J. Alloys Compd. 615 (2018) S676–S679, https://doi.org/10.1016/j.jallcom.2014.05.024.
[66] M.F. Ashby, Materials Selection in Mechanical Design, 5th edition Butterworth-Heinemann, 2016.
[67] Y. Abd-elrhman, M.A.-H. Gepreel, A. Abdel-Moniem, S. Kobayashi, Compatibility assessment of new V-free low-cost Ti–4.7Mo–4.5Fe alloy for some biomedical applications, Mater. Des. 97 (2016) 445–453, https://doi.org/10.1016/j.matdes.2016.02.110.
[68] É.S.N. Lopes, C.A.F. Salvador, D.R. Andrade, A. Cremasco, K.N. Campo, R. Caram, Microstructure, mechanical properties, and electrochemical behavior of Ti-Nb-Fe alloys applied as biomaterials, Metall. Mater. Trans. A 47 (2016) 3213–3226, https://doi.org/10.1007/s11661-016-3411-0.
[69] ASTM International, Standard Specification for Wrought Titanium-12Molybdenum-6Zirconium-2Iron Alloy for Surgical Implant (UNS R58120), Vol. 1, 2013 12–16, https://doi.org/10.1520/F1813-13.2.
[70] Q. Li, M. Niinomi, M. Nakai, Z. Cui, S. Zhu, X. Yang, Effect of Zr on super-elasticity and mechanical properties of Ti–24 at% Nb–(0, 2, 4) at% Zr alloy subjected to aging treatment, Mater. Sci. Eng. A 536 (2012) 197–206, https://doi.org/10.1016/J.MSEA.2011.12.103.